(4)

APPLIED RESEARCH LABORATORY

The Pennsylvania State University
Post Office Box 30
State College, PA 16804

QUARTERLY TECHNICAL PROGRESS REPORT ON FUNDAMENTAL HYDRODYNAMICS RESEARCH (ONR - CODE 12)

1 October 1989 through 31 December 1989

Prepared by Cognizant ARL Penn State Principal Investigators

Garfield Thomas Water Tunnel
Applied Research Laboratory
Penn State University
Post Office Box 30
State College, PA 16804

Telephone: (814) 865-1741

Office of Naval Research
Department of the Navy

Quarterly Technical Progress Report
on Fundamental Hydrodynamics Research
(ONR - Code 12)

1 October 1989 through 31 December 1989

Prepared by Cognizant ARL Penn State
Principal Investigators

Garfield Thomas Water Tunnel
Applied Research Laboratory
The Pennsylvania State University
Post Office Box 30
State College, PA 16804

Telephone: (814) 865-1741

PREFACE

Under the sponsorship of The Office of Naval Research (Code 12) AHR Program, The Applied Research Laboratory of Penn State University performs basic research in hydrodynamics and hydrodynamic noise. The hydrodynamics research conducted under this program falls into two basic thrust areas:

- Turbomachinery

  To develop an improved understanding of the fluid mechanics and acoustics associated with low-speed turbomachines and marine propulsors. To employ this knowledge to the development of improved propulsor and turbomachine design methods.

- Drag Reduction

  To develop fundamental understanding of the mechanisms that cause drag on bodies and surfaces and to explore novel methods to reduce drag.

Under each thrust area, one or more projects are conducted under the direction of the principal investigator who initiated the given task. All tasks are designed to provide results that will improve the scientific understanding of various hydrodynamic phenomena associated with the operation of submerged bodies and surfaces.

This report documents the technical progress realized during the first quarter of FY 90 for the projects currently approved under this program.

TURBOMACHINERY

SUBTASK T1

Title: Turbomachine Internal Flow Definition
(S. A. Abdallah, Cincinnati, and M. L. Billet. Penn State)

BACKGROUND

The internal flow field of a wake adapted turbomachine is dominated by three dimensional and unsteady effects. The three dimensionality of the flow field is demonstrated by the strong secondary flows which have been experimentally measured. The unsteadiness of the flow is due to the interaction of the downstream blade rows with the wakes shed from the upstream blade rows. The development of computational tools to predict accurately these types of flow fields is essential if successful development of high performance turbomachinery is to be achieved.

PROGRESS

In order to participate in the SSPA-CHT-11HR workshop on Ship Viscous Flow, Sweden, 12-14 September 1990, we changed our research goals from unsteady internal flow to steady turbulent flow over a whole ship. The change was approved by Mr. J. Fein.

Preliminary results have been obtained for three-dimensional turbulent flow over a wiggly hull. The Baldwin Lomax turbulence model is used in the calculations. Comparisons with experimental data are in good agreement.

Enclosed is a paper entitled "The Discrete Continuity i: imitive Variable Solutions of Incompressible Flow." Submitted to the Journal of Computational Physics and published in the proceedings of the "Third International Congress of Fluid Mechanics," Cairo, Egypt (Jan. 2-4, 1990).

DRAG REDUCTION

SUBTASK DR1

Title: Turbulent Spot Generation by Freely Suspended Particles
(H. L. Petrie and P. J. Morris)

BACKGROUND

Laminar flow control (LFC) has been an attractive technology for many years but premature transition, induced by particles in the fluid, has prevented its successful hydrodynamic implementation. Although an extensive amount of experimental work and analysis has examined the transition induced by various types of roughness elements and intermittent disturbances such as sparks, basic questions regarding the mechanisms for transition induction by freely suspended particles still remain unanswered. The subject experimental and analytic study of particle induced transition is concerned with these issues and is entering the ninth month of activity.

Heated body LFC experiments have demonstrated clearly the degradation of LFC performance due to freestream particles. However, a detailed explanation of this phenomenon has not been developed. Experiments by Lauchle, et al. [1], observed that nearly neutrally buoyant particles of sufficient size caused turbulent spots on an LFC heated body when seeded into the freestream. However, these particles failed to generated spots when injected through a dye port at the nose of the body. If these particles did not migrate away from the wall significantly while accelerating around the nose, then freestream seeded particles must act on the boundary layer with a different mechanism than the wall injected particles. This suggests that the dynamics of crossing streamlines and possibly wall impact may be crucial to spot formation. In support of this, Hall [2], observed that transition could be induced when a spherical particle supported by wire was pulled into the wall even though, once fixed to the wall, the particle was too small to induce a turbulent spot.

PROGRESS

As reported earlier, the analytical approach is addressing two main issues that support the experimental measurements. The first is the determination of particle trajectories. The second is the calculation of the development of wave packets generated by the moving particles. During this reporting period we have concentrated on two aspects of the analysis related to the trajectory calculations.

The basic flow field has been defined using boundary layer analysis. The Blasius, flat plate boundary layer solution has been matched to second order with the external uniform flow. This solution

includes the external flow due to the displacement thickness of the boundary layer. It also provides a smooth transition for the velocity normal to the wall from its non-zero value at the edge of the boundary layer to its zero value in the freestream. Calculations have been performed for the test conditions to be used in the water channel. The results will be compared with the experimental observations during the calibration phase of the flat plate model.

With the basis defined it is possible to determine particle trajectories. The trajectories depend on the forces acting on the particle. Outside the boundary layer these forces are well understood since the flow is uniform. Particle trajectory calculations are being performed in this region. These will be used to determine the appropriate release location for particles in this experiments. Once the particle enters the boundary layer the situation is more complicated as the basic flow is sheared. In addition to the forces present in the freestream there is a lift force due to the shear and to particle rotation. The proximity of the wall to the particle can also influence the lift. An asymptotic analysis for low particle Reynolds numbers has been performed by Saffman. In fact the lift force has become known as the "Saffman lift force." However, we envision particle Reynolds numbers of the order of 300. Several experiments have been performed to determine the lift force as a function of local shear and distance from the wall. Some experiments involve the direct measurement of lift, which is extremely small. Others involve a balancing of the lift force with buoyancy force in an inclined channel. The uncertainty in the experimental data is quite large. At present we are correlating the data to develop an empirical extension of the Saffman formula to higher Reynolds number. This is in the same spirit as the extension of the Stokes drag coefficient. The separate effects of wall proximity will also be included. This empirical model will be incorporated into the trajectory prediction scheme and predictions will be made for the particle motion within the boundary layer. These predictions will be compared with the particle trajectory measurements when they are available, and modifications, if necessary, will be made to the empirical lift force correlations.

Experiments are to be conducted in the low turbulence open channel flow loop facility of the Aerospace Engineering Department at Penn State. Nearly all of the various pieces for the channel and test plate have been completed. The list of components that have been fabricated or modified includes the test plate with various subassemblies, the channel floor and sidewall support frame, the test section support frame, the diffuser, the settling section inlet, and the flow conditioning section in the settling chamber. This represents a substantial design and fabrication effort that has occupied the time of numerous personnel and is a significant milestone now that we are beginning our ninth month of project activities. Channel assembly and test plate installation will commence early in the next quarter.

Initial familiarization with the computer based video imaging system for particle pathline measurement has begun. To date, this has

been limited to ensuring that all components function as they should and evaluation of the systems software.

PLANS

A major activity of the next quarter will be the installation of the plate, the assembly of the channel and then flowfield evaluation. Initial experimental work will begin late in the quarter with the emphasis being on channel flow quality evaluation. At first, flow visualization will be used to examine the flow from the inlet of the settling chamber to its exit at the test section. The goal of this work is to determine a configuration of the flow conditioning section that is sufficient to quell the large disturbances upstream of it. Following this, the test plate sidewall suction slots and tail must be adjusted. This requires both flow visualization and boundary layer surveys. Coincident with these efforts, imaging techniques, particle release trials, and development of general methodology for the particle experiments will begin. Work on the particle trajectory analysis will continue with the calculations being used as a guide for selection of particle release positions.

REFERENCES

1. Lauchle, G. C., Petrie, H. L., and Stinebring, D. R., "Effects of Particles on the Delayed Transition of a Heated Body," ARL Technical Memorandum 86-213.

2. Hall, W. R., "Interaction of the Wake from Bluff Bodies with an Initially Laminar Boundary Layer," AIAA Journal, V5, N8, pp. 1386-1392. "Boundary Layer on a Flat Plate," Proc. Roy..

SUBTASK DR2

Title: Microbubble Injection in Axisymmetric Flows (S. Deutsch)

BACKGROUND

It has been demonstrated that the injection of gas to form microbubbles in a liquid turbulent boundary layer on a flat plate at nominally zero pressure gradient can reduce skin friction drag by as much as 90% locally. The extension of these results to submerged axisymmetric bodies is the subject of the task.

PROGRESS

A publication based on an extensive set of local skin friction measurements has been accepted (with revision) by the Physics of Fluids. Major results covered in the paper include the fact that the persistence of the phenomenon on an axisymmetric body is the same as that on a flat plate and that the poor performance of microbubble drag reduction at low speeds is a result of a buoyancy driven instability that removes bubbles from the boundary layer.

We are continuing our study of the effect of pressure gradient. We have repeated our integrated skin friction measurements and LDV studies and have measured the pressure gradient on the body with and without bubble injection. Although data analysis is continuing, it appears that the earlier drag reduction data is repeatable and that injection of gas does not change the pressure gradient on the body. Relative levels of drag reduction would appear then to be correct, independent of the effect of pressure gradient on the balance results. Our earlier conclusions that an unfavorable pressure gradient led to higher levels of drag reduction and the prospect of early separation, while a favorable gradient led to much lower levels of drag reduction would appear to be confirmed.

PLANS

Analysis of the LDV data will continue. This should help determine the influence of the pressure gradients on the drag balance results. In addition, we have begun simple computations of the flow field over the axisymmetric body for the zero, adverse and favorable pressure gradient cases. These computations, which employ the measured pressure gradients, will give us yet another test of the reliability of the (absolute) values of the balance results in a pressure gradient.

The results and plans sketched above will provide the basis for a M. S. Thesis in Aerospace Engineering for Mr. H. Clark as well as for an additional publication.

ICFM 3, 1990 1155

THE DISCRETE CONTINUITY IN PRIMITIVE VARIABLE SOLUTIONS OF INCOMPRESSIBLE FLOW

F. Sotiropoulos and S. Abdallah
Department of Aerospace Engineering and Engineering Mechanics
University of Cincinnati, Cincinnati, Ohio U.S.A.

ABSTRACT

The use of a non-staggered computationnal grid for the numerical solutions of the incompressible flow equations has many advantages over the use of a staggered grid. A penalty, however, is inherent in the finite-difference approximations of the governing equations on non-staggered grids. In the primitive-variable solutions, the penalty is that the discrete continuity equation does not converge to a machine accuracy. It rather converges to a source term which is proportional to the fourth order derivative of the pressure, the time increment and the square of the grid spacing. An approach which minimizes the error in the discrete continuity equation is developed. Numerical results obtained for the driven cavity problem confirm the analytical developments.

NOMENCLATURE

D	dilation
ERX, ERY	higher order terms in equations (18a) and (18b) respectively
f, h	variables defined in equations (16a) and (16b) respectively
p	pressure divided by density
Re	Reynolds number
t	time
u,v	velocity components in x- and y-directions respectively
x,y	space coordinates
σ	source term in equation (27)
ξ,η	variables defined in equations (4a) and (4b) respectively
$\delta t, \delta x, \delta y$	time and space increments
δ_x, δ_y	second order accurate finite-difference approximations for the partial derivatives $\partial/\partial x$ and $\partial/\partial y$ respectively
δ_{xx}, δ_{yy}	second order accurate finite-difference approximations for the partial derivatives $\partial^2/\partial x^2$ and $\partial^2/\partial y^2$ respectively.

Subscripts

i,j	refer to grid indices in x- and y-directions respectively.
x,y	refer to partial derivatives with respect to x and y respectively

Superscripts

n	refers to time level t
n+1	refers to time level t+δt

INTRODUCTION

There are two formulations for the numerical solution of the incompressible Navier-Stokes equations in primitive variables; the artificial compressibility and the pressure Poisson methods. In both methods, the velocity field is calculated from the time dependent momentum equation using time marching techniques, while each method employs a different equation to compute the pressure.

In the artificial compressibility method, a time derivative of the pressure is added to the continuity equation [1] and the incompressible field is treated as compressible during the transient calculations. On the other hand, the pressure Poisson method [2] replaces the continuity equation with a second order elliptic Poisson equation for the pressure. The continuity equation is then enforced in the numerics.

An important issue in the numerical solutions of the primitive variable formulations is the satisfaction of the discrete continuity equation when staggered or non-staggered computational grids are used. It has been shown for both methods; the artificial compressibility and the pressure Poisson that the discrete continuity equation is satisfied to a machine zero on staggered grids [2, 3]. Unfortunately, this is not true on non-staggered grids. The artificial compressibility method requires the explicit addition of a fourth order artificial dissipation term to the discrete continuity equation to eliminate odd-even decoupling in the pressure field. The odd-even decoupling is caused by central second order finite-difference approximations of the first order continuity equation. Therefore the discrete divergence of the velocity field is not driven to a machine zero but rather to a term proportional to the fourth order derivative of the pressure [4]. Similarly, the pressure Poisson formulation does not satisfy the discrete continuity equation exactly on non-staggered grids. This phenomenon can be explained by investigating the discrete pressure equation which can be obtained by:

1. Discretization of the continuum pressure Poisson equation using central second order accurate formulas [5, 6].

2. Direct derivation from the discrete divergence of the discrete momentum equation [2].

Although the above approaches lead to the same discrete pressure equation on a staggered grid, they do not give the same equation on non-staggered grids.

Careful examination of the two forms of the discrete pressure equation shows that the direct derivation of the discrete pressure equation satisfies the discrete continuity exactly but fails to give smooth pressure field. The oscillatory behavior of the pressure is caused by the odd-even decoupling inherented in the resulting discrete pressure equation. On the other hand, the first approach gives smooth pressure field, but has two major problems:

1. The compatibility condition of the Poisson Neumann problem is not automatically satisfied.

2. The discrete continuity equation is not exactly satisfied.

The first problem has been resolved in reference [5]. The use of the consistent finite-difference method of Abdallah [5] satisfies the compatibility condition exactly on non-staggered grids. The second problem is the subject of this paper. More specifically, we discuss the reasons which prevent the discrete divergence of the velocity from going to zero and we derive the correct [illegible] discrete continuity [illegible]

MATHEMATICAL FORMULATION

Governing Equations

The equations which govern the laminar, incompressible flow of a Newtonian fluid are given in Cartesian coordinates as follows:

Continuity

$$\frac{\partial u}{\partial x} + \frac{\partial v}{\partial y} = 0 \tag{1}$$

x-Momentum

$$\frac{\partial u}{\partial t} + u\frac{\partial u}{\partial x} + v\frac{\partial u}{\partial y} = -\frac{\partial p}{\partial x} + \frac{1}{Re}\left(\frac{\partial^2 u}{\partial x^2} + \frac{\partial^2 u}{\partial y^2}\right) \tag{2}$$

y-Momentum

$$\frac{\partial v}{\partial t} + u\frac{\partial v}{\partial x} + v\frac{\partial v}{\partial y} = -\frac{\partial p}{\partial y} + \frac{1}{Re}\left(\frac{\partial^2 v}{\partial x^2} + \frac{\partial^2 v}{\partial y^2}\right) \tag{3}$$

where u and v are the velocity components in the x- and y-directions respectively, p is the static pressure divided by the density and Re is the Reynolds number.

The main difficulty associated with the solution of the system (1)-(3) is the continuity equation (1). Equation (1) is a constraint which the velocity field has to satisfy at any instant in time and not an evolution equation of the type (2) or (3). Also, equation (1) does not involve the pressure, which appears only in the momentum equations (2) and (3).

A numerical solution for equations (1)-(3) must incorporate a procedure for taking into account the important interaction between the pressure and velocity fields. In order to achieve this coupling between the pressure and the velocity fields, the continuity equation (1) must be replaced by an equation which involves both pressure and velocity and at the same time guarantees the satisfaction of the incompressibility constraint.

The Pressure Poisson Formulation

In the pressure Poisson formulation, a second-order elliptic equation of Poisson type, for the pressure is derived by applying the divergence operator to the momentum equation :

$$\frac{\partial^2 p}{\partial x^2} + \frac{\partial^2 p}{\partial y^2} = -\left(\frac{\partial \xi}{\partial x} + \frac{\partial \eta}{\partial y}\right) + \frac{\partial D}{\partial t} \tag{4}$$

where

$$\xi = u\frac{\partial u}{\partial x} + v\frac{\partial u}{\partial y} - \frac{1}{Re}\left(\frac{\partial^2 u}{\partial x^2} + \frac{\partial^2 u}{\partial y^2}\right) \tag{4a}$$

$$\eta = u\frac{\partial v}{\partial x} + v\frac{\partial v}{\partial y} - \frac{1}{Re}\left(\frac{\partial^2 v}{\partial x^2} + \frac{\partial^2 v}{\partial y^2}\right) \tag{4b}$$

$$D = \frac{\partial u}{\partial x} + \frac{\partial v}{\partial y} \tag{4c}$$

Up to this point the continuity equation (1) has not been used in the derivation of equation (4). In other words the solution of equation (4) for the pressure, along with equations (2) and (3) for the velocity field, does not guarantee in any way that the computed velocity field will be divergence-free.

To satisfy the continuity equation (1), the time dependent term in the right hand side of equation (4) is discretized in time as follows:

$$\frac{\partial D}{\partial t} = \frac{D(t+\Delta t) - D(t)}{\Delta t} \tag{5}$$

where Δt is the time increment. As suggested by Harlow and Welch [2], the dilation at the $(t+\Delta t)$ time level is set to zero, in order to enforce the continuity equation, while the dilation at the (t) time level is retained. Thus, equation (5) reduces to:

$$\frac{\partial D}{\partial t} = -\frac{D(t)}{\Delta t} \tag{6}$$

It is important to stress here that the same temporal discretization must be used for the unsteady terms in the momentum equations (2) and (3). By incorporating equation (6) into equation (4), we obtain:

$$\frac{\partial^2 P}{\partial x^2} + \frac{\partial^2 P}{\partial y^2} = -\left(\frac{\partial f}{\partial x} + \frac{\partial g}{\partial y}\right) + \frac{D(t)}{\Delta t} \tag{7}$$

Equation (7) is the pressure Poisson equation which has been used by researchers to resolve incompressible flows on staggered [2] and non-staggered grids [6,8]. To see how the solution of equation (7) guarantees the satisfaction of the continuity equation at convergence we should compare equation (4) with equation (7). This comparison reveals that the pressure Poisson equation (7) can be viewed as an evolution equation for the dilation D, namely equation (6). Moreover, the solution of equation (6) is an exponential decay in time, as follows:

$$D(t) = D_o\, e^{-t/\Delta t} \tag{8}$$

where D_o is the initial dilation. Thus, the solution of equation (7) for the pressure, along with equations (2) and (3) for u and v, guarantees that the initial dilation D_o will decay to zero as $t \to \infty$ (i.e. as a steady state is approached). We will not pursue further the analysis of the relation between the pressure and the continuity equations in continuum form - a subject which has been investigated by Gresho and Sani [7].

Discretization of the Governing Equations:

Using the Euler-explicit temporal discretization scheme for the time derivatives and central second order accurate finite difference formulas for the spatial derivatives, the system of the governing equations (7), (2) and (3) can be discretized as follows (see Fig. 1):

$$\frac{P^n_{i+1,j} - 2P^n_{i,j} + P^n_{i-1,j}}{\Delta x^2} + \frac{P^n_{i,j+1} - 2P^n_{i,j} + P^n_{i,j-1}}{\Delta y^2}$$

$$= -\left(\frac{f^n_{i+1/2,j} - f^n_{i-1/2,j}}{\Delta x} + \frac{g^n_{i,j+1/2} - g^n_{i,j-1/2}}{\Delta y}\right) + \frac{D^n_{i,j}}{\Delta t}$$

Up to this point the continuity equation (1) has not been used in the derivation of equation (4). In other words the solution of equation (4) for the pressure, along with equations (2) and (3) for the velocity field, does not guarantee in any way that the computed velocity field will be divergence-free.

To satisfy the continuity equation (1), the time dependent term in the right hand side of equation (4) is discretized in time as follows:

$$\frac{\partial D}{\partial t} = \frac{D(t+\Delta t) - D(t)}{\Delta t} \tag{5}$$

where Δt is the time increment. As suggested by Harlow and Welch [2], the dilation at the $(t+\Delta t)$ time level is set to zero, in order to enforce the continuity equation, while the dilation at the (t) time level is retained. Thus, equation (5) reduces to:

$$\frac{\partial D}{\partial t} = -\frac{D(t)}{\Delta t} \tag{6}$$

It is important to stress here that the same temporal discretization must be used for the unsteady terms in the momentum equations (2) and (3). By incorporating equation (6) into equation (4), we obtain:

$$\frac{\partial^2 p}{\partial x^2} + \frac{\partial^2 p}{\partial y^2} = -\rho\left(\frac{\partial f}{\partial x} + \frac{\partial g}{\partial y}\right) + \frac{D(t)}{\Delta t} \tag{7}$$

Equation (7) is the pressure Poisson equation which has been used by researchers to resolve incompressible flows on staggered [2] and non-staggered grids [6,8]. To see how the solution of equation (7) guarantees the satisfaction of the continuity equation at convergence we should compare equation (4) with equation (7). This comparison reveals that the pressure Poisson equation (7) can be viewed as an evolution equation for the dilation D, namely equation (6). Moreover, the solution of equation (6) is an exponential decay in time, as follows:

$$D(t) = D_o\, e^{-t/\Delta t} \tag{8}$$

where D_o is the initial dilation. Thus, the solution of equation (7) for the pressure, along with equations (2) and (3) for u and v, guarantees that the initial dilation D_o will decay to zero as $t \to \infty$ (i.e. as a steady state is approached). We will not pursue further the analysis of the relation between the pressure and the continuity equations in continuum form - a subject which has been investigated by Gresho and Sani [7].

Discretization of the Governing Equations:

Using the Euler-explicit temporal discretization scheme for the time derivatives and central second order accurate finite difference formulas for the spatial derivatives, the system of the governing equations (7), (2) and (3) can be discretized as follows (see Fig. 1):

$$\frac{p^n_{i+1,j} - 2p^n_{i,j} + p^n_{i-1,j}}{\Delta x^2} + \frac{p^n_{i,j+1} - 2p^n_{i,j} + p^n_{i,j-1}}{\Delta y^2}$$

$$= -\rho\left(\frac{f^n_{i+1/2,j} - f^n_{i-1/2,j}}{\Delta x} + \frac{g^n_{i,j+1/2} - g^n_{i,j-1/2}}{\Delta y}\right) + \frac{D^n_{i,j}}{\Delta t}$$

$$u_{i,j}^{n+1} = u_{i,j}^{n} - \Delta t \left(\frac{P_{i+1,j}^{n} - P_{i-1,j}^{n}}{2\Delta x} + \xi_{i,j}^{n}\right) \tag{10}$$

$$v_{i,j}^{n+1} = v_{i,j}^{n} - \Delta t \left(\frac{P_{i,j+1}^{n} - P_{i,j-1}^{n}}{2\Delta y} + \eta_{i,j}^{n}\right) \tag{11}$$

where

$$\xi_{i,j} = [u_{i,j}\delta_x + v_{i,j}\delta_y - \frac{1}{Re}(\delta_{xx} + \delta_{yy})]u_{i,j} \tag{12a}$$

$$\eta_{i,j} = [u_{i,j}\delta_x + v_{i,j}\delta_y - \frac{1}{Re}(\delta_{xx} + \delta_{yy})]v_{i,j} \tag{12b}$$

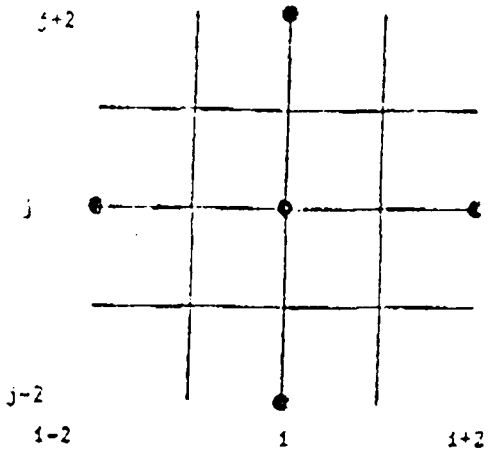

Fig. 1. Finite Difference Grid.

The first and second order operators (δ_x, δ_y) and $(\delta_{xx}, \delta_{yy})$ are the central second order finite-difference approximations for the $(\frac{\partial}{\partial x}, \frac{\partial}{\partial y})$ and $(\frac{\partial^2}{\partial x^2}, \frac{\partial^2}{\partial y^2})$ derivatives, respectively. The pressure equation was discretized according to the consistent finite difference method proposed by Abdallah [6].

Equation (9) is solved for $P_{i,j}^{n}$, given $u_{j,j}^{n}$ and $v_{i,j}^{n}$, and then the velocity field is updated using equations (10) and (11). At this point of our discussion, it seems important to pose the following question: Does the solution of equations (9), (10) and (11) guarantee that the computed velocity field will be divergence free in the discrete computational space? In order to answer this question, we should first understand how the discrete continuity equation is modeled in the pressure equation (9). This point can be made very clear if we look at the derivation of equation (9) from a different point of view. Let us consider the following discrete approximation of the continuity equation (1) which we seek to satisfy at the time level t+Δt (n+1):

$$\frac{u_{i-1/2,j}^{n+1} - u_{i-1/2,j}^{n+1}}{\Delta x} + \frac{v_{i,j+1/2}^{n+1} - v_{i,j-1/2}^{n+1}}{\Delta y} = 0 \tag{13}$$

The pressure Poisson equation (9) can be derived from equation (13) if we employ the x- and y-momentum equations at the nodes (i±1/2,j) and (i,j±1/2). Expressions for $u^{n+1}_{i\pm1/2,j}$ and $v^{n+1}_{i,j\pm1/2}$ are obtained as follows:

$$u^{n+1}_{i\pm1/2,j} = u^{n}_{i\pm1/2,j} - \Delta t \left(\pm \frac{P_{i\pm1,j}-P_{i,j}}{\Delta x} + \xi_{i\pm1/2,j}\right)^{n} \tag{14a}$$

$$v^{n+1}_{i,j\pm1/2} = v^{n}_{i,j\pm1/2} - \Delta t \left(\pm \frac{P_{i,j\pm1}-P_{i,j}}{\Delta y} + \eta_{i,j\pm1/2}\right)^{n} \tag{14b}$$

Substituting equations (14a) and (14b) into equation (13) we obtain:

$$\frac{1}{\Delta x}\left[\left(\frac{P_{i+1,j}-P_{i,j}}{\Delta x} + \xi_{i+1/2,j}\right) - \left(\frac{P_{i,j}-P_{i-1,j}}{\Delta x} + \xi_{i-1/2,j}\right)\right]^{n}$$

$$+ \frac{1}{\Delta y}\left[\left(\frac{P_{i,j+1}-P_{i,j}}{\Delta y} + \eta_{i,j+1/2}\right) - \left(\frac{P_{i,j}-P_{i,j-1}}{\Delta x} + \eta_{i,j-1/2}\right)\right]^{n}$$

$$= \frac{1}{\Delta t}\left[\frac{u_{i+1/2,j}-u_{i-1/2,j}}{\Delta x} + \frac{v_{i,j+1/2}-v_{i,j-1/2}}{\Delta y}\right]^{n} \tag{15}$$

It takes some simple algebra to show that equation (15) is identical to equation (9). Notice, that the right hand side of equation (15) is the divergence of the velocity field while its left hand side consists of the x- and y- components of the steady state form of the momentum equation, computed at the nodes (i±1/2,j) and (i,j±1/2) respectively. Thus, if the momentum equations are driven to steady state at these nodes, the left hand side of equation (15) eventually approaches zero and so does the divergence of the velocity field. Unfortunately, on a non-staggered grid, the momentum equations are not driven to zero at (i±1/2,j) and (i,j±1/2) nodes but they are at the (i,j) nodes (see equations (10) and (11)). This inconsistency between the discrete momentum and continuity equations prevents the discrete divergence of the velocity (right hand side of equation (15)) from approaching zero. This observation, raises the following question: what is the size of the mass source (error in D) which equation (15) introduces into the flow field? We answer this question in the following section.

Estimation of the Error in the Discrete Continuity

To simplify the algebra, we perform the following analysis using the Euler rather than the Navier-Stokes equations. So, we drop the viscous terms from equations (9), (10) and (11). This simplification does not alter significantly the generality of our results.

For the sake of convenience, let us introduce the following notations:

$$f = \frac{\partial P}{\partial x} + u\frac{\partial u}{\partial x} + v\frac{\partial v}{\partial y} \tag{16a}$$

and

$$h = \frac{\partial P}{\partial y} + u\frac{\partial v}{\partial x} + v\frac{\partial v}{\partial y} \tag{16b}$$

Using the above notations, the pressure equation (9) (or (15)) can be written as follows:

$$\frac{f^{n}_{i+1/2,j} - f^{n}_{i-1/2,j}}{\Delta x} + \frac{h^{n}_{i,j+1/2} - h^{n}_{i,j-1/2}}{\Delta y} = \frac{D^{n}_{i,j}}{\Delta t} \tag{17}$$

To express $f_{i\pm1/2,j}$ and $h_{i,j\pm1/2}$ in terms of $f_{i,j}$ and $h_{i,j}$, we use Taylor series expansion around the points $(i\pm1/2,j)$ and $(i,j\pm1/2)$ respectively.

With reference to Fig. 1, we obtain:

$$f_{i\pm1/2,j} = \frac{1}{2}\,(f_{i\pm1,j} + f_{i,j}) + ERX^{\pm} \tag{18a}$$

$$h_{i,j\pm1/2} = \frac{1}{2}\,(h_{i,j\pm1} + h_{i,j}) + ERY^{\pm} \tag{18b}$$

where ERX and ERY contain the higher order terms of the series. These terms can be expressed in terms of the primitive variables u, v and p using equations (16a) and (16b) for f and h. But first let us rewrite equations (18) as

$$ERX^{\pm} = f_{i\pm1/2,j} - \frac{1}{2}\,(f_{i\pm1,j} + f_{i,j}) \tag{19a}$$

$$ERY^{\pm} = h_{i,j\pm1/2} - \frac{1}{2}\,(h_{i,j\pm1} + h_{i,j}) \tag{19b}$$

By substituting the finite-difference approximations of f and h in equation (19), one obtains

$$\begin{aligned} ERX^{\pm} = {} & \pm\tfrac{1}{4}\,u_{i\pm1,j}\,(u_{i\pm2,j} - 2u_{i\pm1,j} + u_{i,j})/4\Delta x \\ & \pm u_{i,j}\,(u_{i+1,j} - 2u_{i,j} + u_{i-1,j})/4\Delta x \\ & + v_{i,j}\,(u_{i\pm1,j+1} - u_{i\pm1,j-1} - u_{i,j+1} + u_{i,j-1})/8\Delta y \\ & + v_{i\pm1,j}\,(-u_{i\pm1,j+1} + u_{i\pm1,j-1} + u_{i,j+1} - u_{i,j-1})/8\Delta x \\ & \pm\tfrac{1}{4}\,(P_{i\pm2,j} - 3P_{i\pm1,j} + 3P_{i,j} - P_{i\pm1,j})/4\Delta x \end{aligned} \tag{20}$$

A similar expression for $ERY^{\pm}$ can be obtained using the same method.

As the solution of the system of equations (10), (11) and (17) approaches the steady state solution, the values of $f_{i,j}$ and $h_{i,j}$ approach zero at all the grid points (i,j). Then equations (18) reduce to

$$f_{i\pm1/2,j} = ERX^{\pm} \tag{21a}$$

$$h_{i,j\pm1/2} = ERY^{\pm} \tag{21b}$$

Upon substitution of equations (21) into equation (17), we obtain the steady state value of the dilation

$$D_{i,j} = \Delta t\,\left(\frac{ERX^{+} - ERX^{-}}{\Delta x} + \frac{ERY^{+} - ERY^{-}}{\Delta y}\right) \tag{22}$$

In order to express $D_{i,j}$ in terms of the dependent variables u, v and p, we incorporate equation (20) and the similarly derived equation for $ERY^{\frac{1}{2}}$ into equation (22).

$$D_{i,j} = -\frac{\Delta t}{4}\{\Delta x^2\,\delta_{xxxx}P + \Delta y^2\,\delta_{yyyy}P + \Delta x^2\,\delta_{xx}(u\,\delta_{xx}u) + \Delta y^2\,\delta_{yy}(v\,\delta_{yy}v) + \text{cross derivative terms}\} \tag{23}$$

where

$$\delta_{xxxx}P = (P_{i+2,j} - 4P_{i+1,j} + 6P_{i,j} - 4P_{i-1,j} + P_{i-2,j})/\Delta x^4 \tag{23a}$$

and

$$\delta_{yyyy}P = (P_{i,j+2} - 4P_{i,j+1} + 6P_{i,j} - 4P_{i,j-1} + P_{i,j-2})/\Delta y^4 \tag{23b}$$

The right hand side of equation (23) is the mass source (error in the discrete continuity) which is introduced into the flow field when equation (9) is used to compute the pressure. Clearly, on a non-staggered grid the discrete continuity is satisfied up to a term proportional to the fourth order spatial derivatives of the pressure and the velocity components. We should mention here that the inclusion of the viscous terms in our analysis would have only introduced higher order terms in equation (22) without altering its generality. In any case, the contribution of the viscous terms decreases as the Reynolds number increases.

Equation (22) reveals the following very interesting aspects of the pressure Poisson formulation on a non-staggered grid:

i) The pressure Poisson method satisfies the discrete continuity equation almost to the same accuracy as the artificial compressibility method does. Recall that a fourth order artificial dissipation term is explicitly added to the pseudo-compressible continuity equation of the artificial compressibility method [4], to stabilize the numerical solution. In the pressure Poisson formulation, the artificial dissipation is "implicitly" added to the continuity equation because of the way the pressure equation is discretized on a non-staggered grid.

ii) Our experience with the pressure Poisson method [6, 8] and other researchers' experience with the artificial compressibility method [4] show that the dilation can be quite large in regions of the flow field where high pressure gradients occur. High pressure gradients result in high values of the fourth order pressure derivatives (artificial dissipation term) and thus, a significant mass source is generated in the continuity equation. Fortunately, the dilation in the Poisson formulation is explicitly dependent on the square of the grid spacing and the time increment. Therefore, to control the errors in the discrete continuity, we strongly recommend the use of fine grid in the regions of high pressure gradients.

Direct Derivation of the Discrete Pressure Equation

The previous discussion suggests that, in order to satisfy the discrete continuity equation, the pressure equation should be derived from the following discrete approximation of equation (

and p. we

$$\frac{u^{n+1}_{j+1,j} - u^{n+1}_{j-1,j}}{2\Delta x} + \frac{v^{n+1}_{i,i+1} - v^{n+1}_{i,j-1}}{2\Delta y} = 0 \qquad (24)$$

into

Using equations (10) and (11) into equation (24) we obtain the following discrete pressure equation:

$$\frac{1}{2\Delta x}\left[\left(\frac{P_{i+2,j}-P_{i,j}}{2\Delta x} + \xi_{i+1,j}\right) - \left(\frac{P_{i,j}-P_{i-2,j}}{2\Delta x} + \eta_{i-1,j}\right)\right]^n$$

$$+ \frac{1}{2\Delta y}\left[\left(\frac{P_{i,j+2}-P_{i,j}}{2\Delta y} + \eta_{i,j+1}\right) - \left(\frac{P_{i,j}-P_{i,j-2}}{2\Delta y} + \eta_{i,j-1}\right)\right]^n \qquad (25a)$$

$$= \frac{1}{\Delta t} D^n_{i,j}$$

(23) (23a)

or

$$\frac{P^n_{i+2,j} - 2P^n_{i,j} + P^n_{i-2,j}}{4\Delta x^2} + \frac{P^n_{i,j+2} - 2P^n_{i,j} + P^n_{i,j-2}}{4\Delta y^2}$$

(23b)

$$= -\left(\frac{\xi^n_{i+1,j} - \xi^n_{i-1,j}}{2\Delta x} + \frac{\eta^n_{i,j+1} - \eta^n_{i,j-1}}{2\Delta y}\right) + \frac{D^n_{i,j}}{\Delta t} \qquad (25b)$$

the
ion (9)
discrete
ential
ion here

By inspecting equation (25a), we can easily conclude that, at convergence, its left hand side will be driven to zero since it involves the steady state form of the x- and y-momentum equations at nodes where they are driven to zero. Therefore, equation (25) will satisfy the discrete continuity equation to a machine zero.

erality.
holds

Unfortunately, the discrete pressure equation (25) produces oscillatory solutions for the pressure because of odd-even decoupling. This can be clearly seen by inspecting the discrete Laplace operator in the left hand side of equation (25) which contains either odd or even grid points in the x- or y-direction. Therefore, in two-dimensions equation (25) gives decoupled solutions for the pressure on the odd-odd, even-even, odd-even and even-odd grid points. Each solution is a unique solution for the pressure within an arbitrary constant. Interestingly, the odd-odd solution, for example, is actually a solution for the pressure equation on a staggered grid which is a subset of the original non-staggered grid (see Fig. 2). Similar conclusions can be drawn about the other three solutions.

tion
d does
y added

n the
itly"
uation

[4] show
here
gh
ion
uity

lity, we
ure

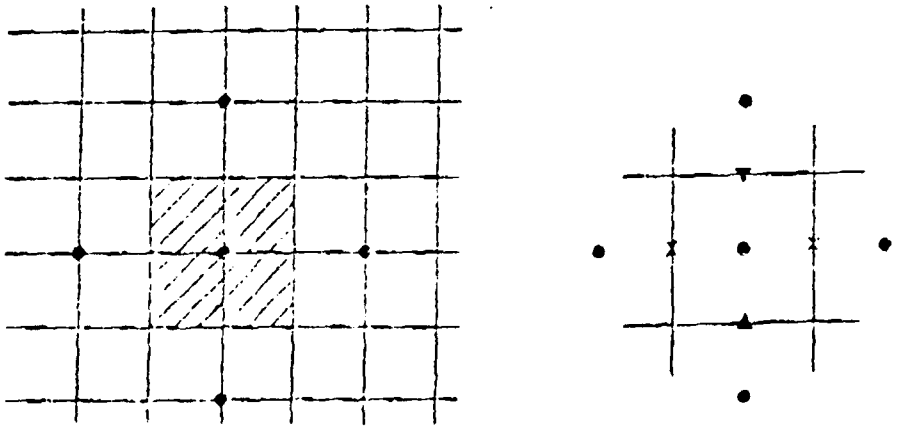

to
lowing

Fig. 2. Equivalence Between Odd-Odd Points and Staggered Grid

In conclusion, the use of equation (9) to compute the pressure will produce a smooth pressure field, but it will not satisfy the discrete continuity equation exactly. While the use of equation (25) will produce exactly the opposite result. In other words, on a non-staggered grid it is not possible to satisfy the discrete continuity to a machine zero and, at the same time, obtain a smooth pressure field. In general, one has to sacrifice partially the satisfaction of the discrete continuity since a smooth and physically meaningful pressure field is desired.

In order to modify equation (25) so that it produces smooth pressure field, we must set aside the idea of satisfying the discrete continuity to machine accuracy. More specifically, we seek to satisfy the discrete continuity up to a fraction of the mass source of equation (22), as follows:

$$\frac{u^{n+1}_{i+1,j} - u^{n+1}_{i-1,j}}{2\Delta x} + \frac{v^{n+1}_{i,j+1} - v^{n+1}_{i,j-1}}{2\Delta y}$$

$$= -\epsilon \frac{\Delta t}{4} \left[\Delta x^2 \delta_{xxxx}(P^n_{i,j}) + \Delta y^2 \delta_{yyyy}(P^n_{i,j})\right] \qquad (26)$$

where ϵ is a positive constant ($0 \le \epsilon \le 1$). Using the momentum equations (10) and (11) into (25), we obtain the following discrete pressure equation:

$$\frac{P_{i+2,j} - 2P_{i,j} + P_{i-2,j}}{4\Delta x^2} + \frac{P_{i,j+2} - 2P_{i,j} + P_{i,j-2}}{4\Delta y^2} - \frac{\epsilon}{4}\left[\Delta x^2 \delta_{xxxx} + \Delta y^2 \delta_{yyyy}\right] P^n_{i,j}$$

$$= -\sigma^n_{i,j} + \frac{D^n_{i,j}}{\Delta t} \qquad (27)$$

where

$$\sigma_{i,j} = \frac{\xi_{i+1,j} - \xi_{i-1,j}}{2\Delta x} + \frac{\eta_{i,j+1} - \eta_{i,j-1}}{2\Delta y}$$

It is interesting to note that for $\epsilon = 0$ equation (27) reduces to equation (24) while for $\epsilon = 1$ the left hand side of equation (27) reduces to the left hand side of equation (9). Furthermore, both equations (27) and (9) produce a smooth pressure field but they fail to satisfy the discrete continuity to a machine zero. However, the error in the discrete continuity which is produced by equation (27) is much less than that produced by equation (9), because:

(i) There is no error contribution to the mass source (compare equations (22) and (26)) from the source term of the pressure equation (27).

(ii) Numerical experiments show that the odd-even decoupling can be removed by using numerical values for $\epsilon \ll 1$ (see results and discussion section).

Another advantage that equation (27) has over equation (9) is associated with the computational work (CPU time) required to advance the pressure and velocity fields to the new time level. When equation (9) is solved for P along with equations (10) and (11) for u and v, the ξ and η terms need to be discretized twice every time step at $(i\pm1/2, j\pm1/2)$ for the pressure equation and at $(i\pm1, j\pm1)$ for the momentum equations. This is not the case when equation (27) is used, since both the pressure and momentum equations require the calculation of the ξ and η terms at the same nodes. Therefore, we recommend the use of equation (27) in the pressure Poisson formulations on non-staggered grids, since it minimizes the error in the discrete continuity ($\epsilon \ll 1$) and reduces the computational time in the numerical solutions.

Boundary Conditions for the Pressure Equation:

Neumann boundary conditions for the pressure Poisson equation are obtained using the normal component of the momentum equation along the boundary contour. For example, at a boundary x-constant:

$$\frac{\partial P}{\partial x} = - u \frac{\partial u}{\partial x} - v \frac{\partial u}{\partial y} + \frac{1}{Re} \left(\frac{\partial^2 u}{\partial x^2} + \frac{\partial^2 u}{\partial y^2} \right) \tag{28}$$

The boundary condition (28) is applied at one half grid spacing away from the boundary for equation (9) [5]. In the case of equation (25) the boundary condition (28) is applied at the boundary using one sided finite difference approximations for the x-derivatives.

The Compatibility Condition

The boundary value problem, consisting of the pressure Poisson equation and the Neumann boundary conditions, has a unique solution if and only if the following integral constraint is satisfied:

$$\iint_A \left(- \frac{\partial f}{\partial x} - \frac{\partial h}{\partial y} + \frac{D}{\Delta t} \right) dA = \int_S \frac{\partial P}{\partial n} ds \tag{29}$$

where n is the outward unit vector normal to the boundary contour S enclosing the solution domain A. Equation (9) satisfies identically the compatibility condition on a non-staggered grid [5]. We will show that equation (25) satisfies the integral constraint (29) as well.

For the sake of convenience we use the notation introduced in equations (16a) and (16b). Incorporating equations (16) into (27) we obtain:

$$\frac{f_{i+1,j} - f_{i-1,j}}{2\Delta x} + \frac{h_{i,j+1} - h_{i,j-1}}{2\Delta y} - \frac{\epsilon}{4} \left[\Delta x^2 \delta_{xxxx} + \Delta y^2 \delta_{yyyy} \right] P_{i,j} = \frac{D_{i,j}}{\Delta t} \tag{30}$$

The discrete form of the integral constraint (29) when applied to equation (30), reads as follows:

$$\sum_{i=2}^{im-1} \sum_{j=2}^{jm-1} \left(\frac{f_{i+1,j} - f_{i-1,j}}{2\Delta x} + \frac{h_{i,j+1} - h_{i,j-1}}{2\Delta y} \right.$$

$$\left. - \frac{\epsilon}{4} \left[\Delta x^2 \delta_{xxxx} + \Delta y^2 \delta_{yyyy} \right] P_{i,j} - \frac{D_{i,j}}{\Delta t} \right) = 0 \tag{31}$$

where im and jm are the numbers of the maximum grid points in the x- and y-directions respectively. Equation (31) can be simplified as follows:

$$\sum_{j=2}^{jm-1} \left(f_{im-1,j} + f_{im-1,j} - f_{2,j} - f_{1,j} \right) + \sum_{i=2}^{im-1} \left(h_{i,jm} + h_{i,jm-1} - h_{i,2} - h_{i,1} \right)$$

$$- \sum_{i=2}^{im-1} \sum_{j=2}^{jm-1} \left(\frac{\epsilon}{4} \left(\Delta x^2 \delta_{xxxx} + \Delta y^2 \delta_{yyyy} \right) P_{i,j} + \frac{D_{i,j}}{\Delta t} \right) = 0 \tag{32}$$

Applying the Neumann boundary conditions at i=1 and im ($f_{1,j} = f_{im,j} = 0$) and at j=1 and jm ($h_{i,1} = h_{i,jm} = 0$) and noting that $f_{2,j} = f_{im-1,j} = h_{i,2} = h_{i,jm-1} = 0$ at steady state we can easily see that the first two terms in equation (32) vanish

identically. Finally, the third term in equation (32) is also zero since the "continuity" equation is locally satisfied at every node. Therefore, equation (32) and consequently equation (31) are identically satisfied on a non-staggered grid.

RESULTS AND DISCUSSION

The driven cavity problem is selected here as the model problem to confirm our analytical developments. Numerical solutions for the momentum equations (10) and (11) are obtained using the Euler explicit scheme and the pressure Poisson equation using the successive over-relaxation method. Both forms of the discrete pressure equations (9) and (27) are used to investigate their ability to satisfy the discrete continuity.

All calculations are performed on uniform non-staggered grids starting from the initial conditions $u_{i,j} = x_{i,j}$, $v_{i,j} = y_{i,j}$ and $P_{i,j} = 0$. The reason for this choice is that we want to explore the capability of the pressure Poisson method to decay an initially high dilation.

The first numerical experiment is conducted on a (31x31) grid using equation (27) as the discrete pressure equation. The artificial dissipation parameter ϵ is set to zero. The time evolution of the logarithm of the average dilation at a node is shown in Fig. 3. Clearly the initially high dilation decays to the machine zero (single precision) at steady state. As we expected, the computed velocity field is smooth, while the pressure field is oscillatory because of odd-even decoupling.

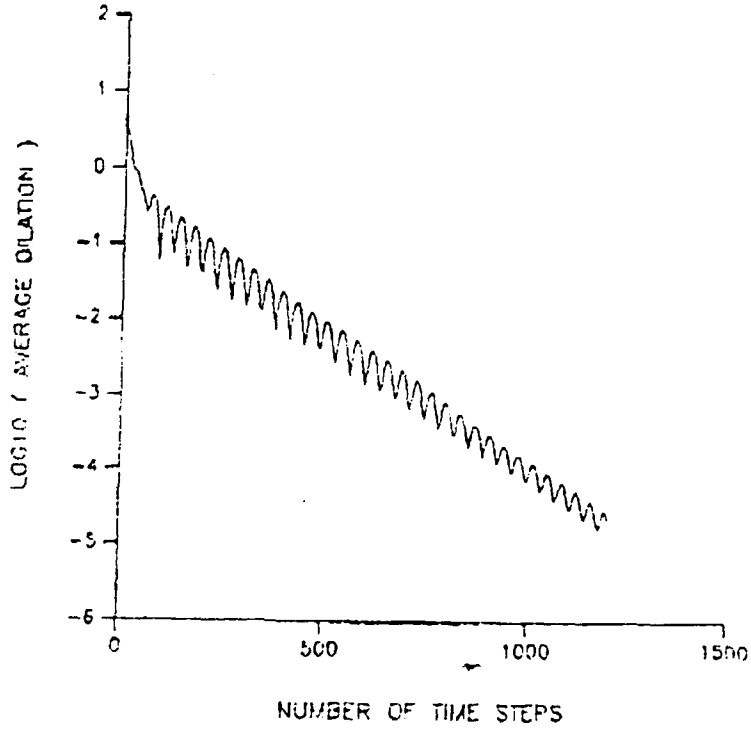

Fig. 3. Convergence of D ($\epsilon = 0$)

To eliminate the decoupling of the pressure modes, we conducted a second experiment on the same grid using equation (27) with non-zero values of ϵ. Our results indicate that values of ϵ as low as 0.1 are sufficient to produce smooth pressure fields. The logarithm of the average dilation at a point is shown in Fig. 4 for $\epsilon = 0.1$. In the same figure it is also shown the dilation when equation (9) is used to compute the pressure on the same grid. As can be seen in Fig. 4, equation (27) with $\epsilon = 0.1$ decays the logarithm of the initial dilation to a steady state value 0.005, while the corresponding value for equation (9) is 0.02. The results confirm our analytical developments since it clearly show that equation (9) produces a higher dilation than equation (27) with $0 \leq \epsilon \leq 1$. We should mention here that the driven cavity problem is particularly difficult case as far as the satisfaction of the discrete continuity is concerned. The reason for that is the existence of high pressure gradients near the moving wall and the two singular corners. The rapid spatial variation of the pressure in that region results in high values of the dilation (at least an order of magnitude higher than the average value). Recall that the steady state value of the dilation depends upon the fourth order derivatives of the pressure.

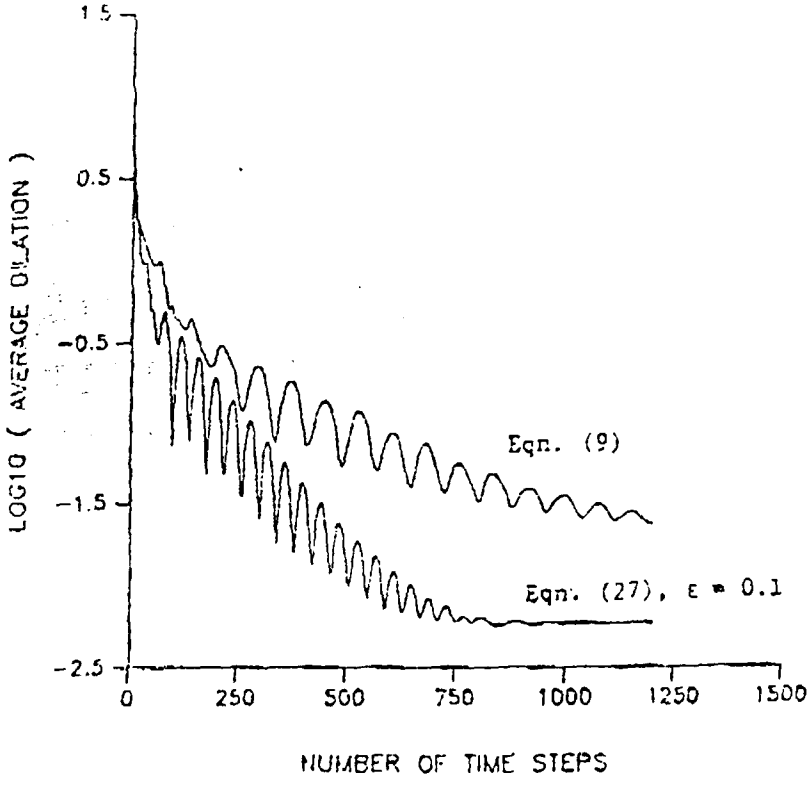

Fig. 4. Convergence for D on a 31x31 Grid.

A third numerical experiment is conducted on a (51x51) grid in order to demonstrate the role of the grid refinement on the discrete continuity. Figure 5 shows the convergence of the dilation for equation (27) with $\epsilon = 0.1$ and equation (9). As expected, equation (27) produces a steady state dilation of 0.0024 while the corresponding value for equation (9) is 0.014. Comparisons of these values with the corresponding ones on the (31x31) grid confirms the dependence of the dilation on the grid spacing, see equation (23)

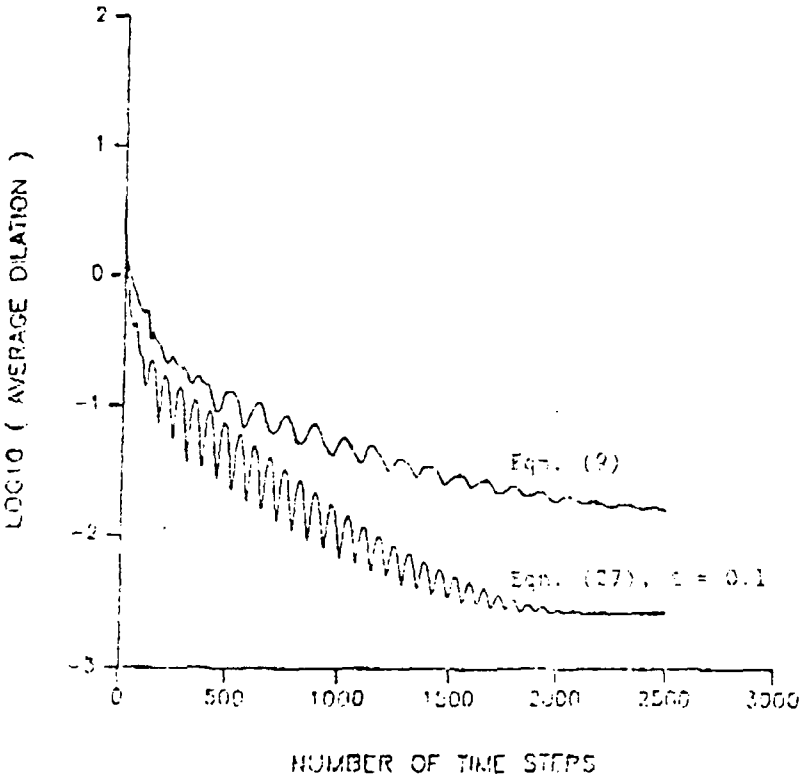

Fig. 5. Convergence for D on 51x51 Grid.

The backward facing step (see Fig. 6) is used as a second test case in order to verify the accuracy of the proposed pressure Poisson solver when analyzing an inflow-outflow problem. We perform laminar calculations over a wide range of Reynolds numbers on a 201x51 uniform grid. The Reynolds number is based on twice the step height and the downstream boundary is located at a - 30h, where h is the step height. The computed reattachment lengths as well as the length of the secondary separation bubble on the upper wall are shown in Figs. 7 and 8, respectively. The comparison with the experimental data of Ref. [9] is very good up to Re = 600. For higher Reynolds numbers, the flow field becomes three dimensional [9] and thus two-dimensional calculations are not sufficient. The same trend has been observed in other two dimensional calculations [10], [11] which are also shown in the same figures.

CONCLUSIONS

We showed that the discrete solutions of incompressible flows, using the classical pressure Poisson formulation on non-staggered grids, do not satisfy the discrete continuity to a machine accuracy. We also showed that the error in the discrete continuity is proportional to the fourth order derivatives of the pressure, the time increment and the square of the grid spacing. It is interesting to point out that the error is proportional to the explicitly added artificial dissipation term in the pseudo-compressibility method. Since the error is dependent upon the time and space increments, it is recommended that a fine grid, in regions of high pressure gradients, to be used in order to minimize the errors in the errors in the discrete continuity

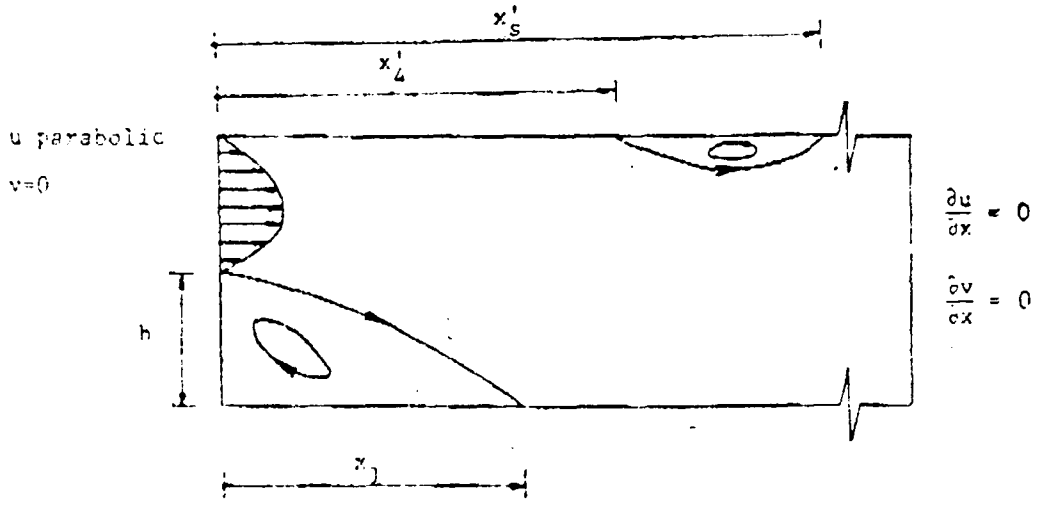

Fig. 6. Backward Facing Step.

order to
cing an
nge of
ed on
, where h
ength of
and 8.
s very
ros three
ct. The
, [11]

ing the
satisfy
error in
of the

tly added
ze the
ed that a
to

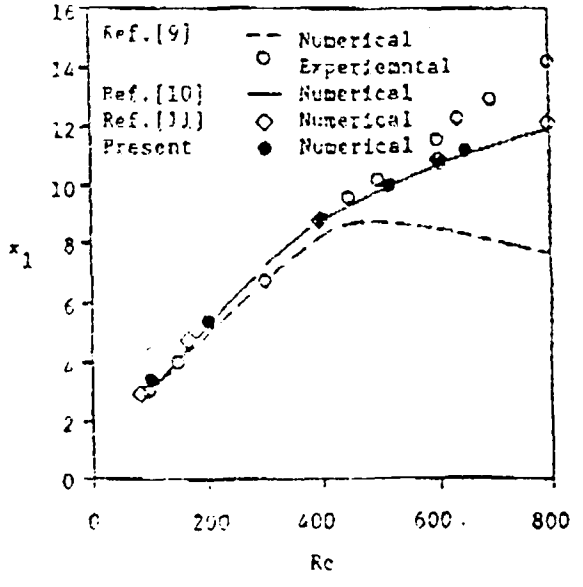

Fig. 7. Reattachment Length As a Function of Re.

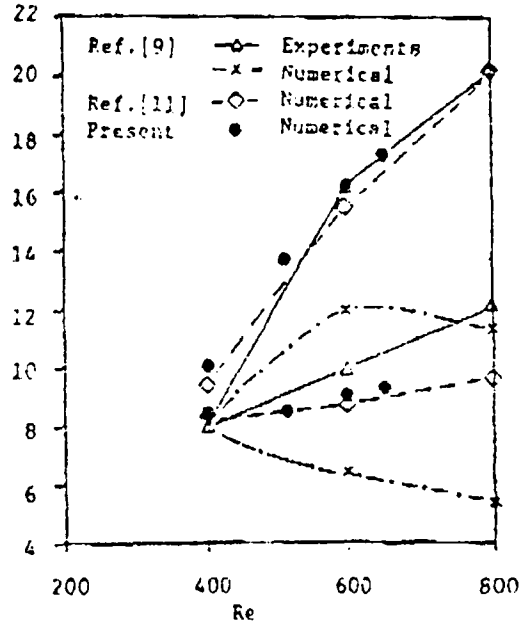

Fig. 8. Length of Secondary Bubble As a Function of Re.

We derived a modified discrete pressure Poisson equation which satisfies the discrete continuity on non-staggered grids up to a fraction of the dissipation term in the classical pressure Poisson formulation. In addition to minimizing the error in the discrete continuity, the method also reduces the computational work required for the discretization of the pressure equation.

ACKNOWLEDGEMENT

This work was sponsored by the Office of Naval Research. The authors thank the Monitor of the program Mr. J. Fein, for the support of this project.

REFERENCES

1. A J. Chorin, J. Comput. Phys. 2, 12 (1967)
2. F.H. Harlow and J.E. Welch, Phys. Fluids 8, 2182 (1965).
3. W.Y. Soh and S.A. Berger, Int. J. Numer. Methods Fluids, Vol. 7, 733-755 (1987).
4. S.E. Rogers, C.C. Boulder, D. Kwak, and U. Kaul, "On the Accuracy of the Pseudocompressibility Method in Solving the Incompressible Navier-Stokes Equations," AIAA 85-1689, presented at the AIAA 18th Fluid Dynamics and Plasmadynamics and Lasers Conference, July 16-18, 1985, Cincinnati, Ohio
5. S. Abdallah, J. Comput. Phys. 70, 182-192 (1987).
6. S. Abdallah, J. Comput. Phys. 70, 193-202 (1987).
7. P.M. Gresho and R.L. Sani, Int. J. Numer. Methods Fluids, 7, 1111-1145 (1987).
8. F. Sotiropoulos and S. Abdallah, J. Comput. Phys. (to appear).
9. B.F. Armaly, F. Durst, and J.C.F. Pereira, J. Fluid Mech., 127 (1983), 473.
10. J. Kim and P. Moin, J. Comput. Phys. 30 (1979), 76.
11. G. Guj and F. Stella, Int. J. Numer. Methods Fluids, 8 (1988), 405.

DISTRIBUTION LIST

Office of Naval Research
800 North Quincy Street
Department of the Navy
Arlington, VA 22217
Attn: A. D. Wood, Code 12
R. J. Hansen, Code 1215
J. A. Fein, Code 1215
M. M. Reischman, Code 11
M. Orr, Code 11250A
E. P. Rood, Code 121132F

Office of Naval Research
Admin. Contracting Officer
The Ohio State University
Research Center
1314 Kinnear Road
Room 318
Columbus, OH 43212-1194
Attn: N. A. Meeks

Office of Naval Technology
800 North Quincy Street
Department of the Navy
Arlington, VA 22217-5000
Attn: A. J. Faulstich, Jr., Code ONT-234
D. C. Houser, Code OCNR-232
C. Votaw, Code OCNR-232

Naval Underwater Systems Center
Newport, RI 02840
Attn: D. J. Goodrich, Code 3634
D. A. Brown, Code 8214

University of Cincinnati
Department of Aerospace Engineering
Cincinnati, OH 45221
Attn: S. A. Abdallah

Applied Research Laboratory
The Pennsylvania State University
Post Office Box 30
State College, PA 16804
Attn: L. R. Hettche
M. L. Billet
S. Deutsch
R. E. Henderson
G. C. Lauchle
P. J. Morris
H. L. Petrie
R. Stern
FDT Files

Director
Naval Research Laboratory
Washington, DC 20375
Attn: Code 2627
(6 Copies)

Defense Technical Information
Center
Building 5
Cameron Station
Alexandria, VA 22314
(12 Copies)

REPORT DOCUMENTATION PAGE

Form Approved
OMB No. 0704-0188

1. AGENCY USE ONLY (Leave blank)	2. REPORT DATE	3. REPORT TYPE AND DATES COVERED
		Quarterly 10/1/89-12/1/89

4. TITLE AND SUBTITLE
FUNDAMENTAL HYDRODYNAMICS RESEARCH

5. FUNDING NUMBERS
N00014-87-K-0196

6. AUTHOR(S)
Abdallah, S. A. and Billet, M. L. - Subtask T1
Petrie, H. L. and Morris, P. J. - Subtask DR1
Deutsch, S. - Subtask DR2

7. PERFORMING ORGANIZATION NAME(S) AND ADDRESS(ES)
Applied Research Laboratory
Penn State University
Post Office Box 30
State College, PA 16804

8. PERFORMING ORGANIZATION REPORT NUMBER

9. SPONSORING/MONITORING AGENCY NAME(S) AND ADDRESS(ES)
Office of Naval Research
800 N. Quincy Street
Department of the Navy
Arlington, VA 22217
Attn: Code 1215

10. SPONSORING/MONITORING AGENCY REPORT NUMBER

11. SUPPLEMENTARY NOTES

12a. DISTRIBUTION/AVAILABILITY STATEMENT
Unclassified/Unlimited

12b. DISTRIBUTION CODE

13. ABSTRACT *(Maximum 200 words)*

Under the sponsorship of the Office of Naval Research (Code 12) AHR Program, the Applied Research Laboratory of Penn State University performs basic research in hydrodynamics and hydrodynamic noise. The hydrodynamics research conducted under this program falls into two basic thrust areas:

·Turbomachinery - To develop an improved understanding of the fluid mechanics and acoustics associated with low-speed turbomachines and marine propulsors. To employ this knowledge to the development of improved propulsor and turbomachine design methods.

·Drag Reduction - To develop fundamental understanding of the mechanisms that cause drag on bodies and surfaces and to explore novel methods to reduce drag.

Under each thrust area, one or more projects are conducted under the direction of the principal investigator who initiated the given task. All tasks are designed to provide results that will improve the scientific understanding of various hydrodynamic phenomena associated with the operation of submerged bodies and surfaces.

This report documents the technical progress realized during the first quarter of FY 90 for the projects currently approved under this program.

14. SUBJECT TERMS
turbomachinery, drag reduction, microbubbles, pressure gradients, particle trajectories, transition, computational fluids, unsteady 3-D flows, turbulent flow

15. NUMBER OF PAGES

16. PRICE CODE

17. SECURITY CLASSIFICATION OF REPORT	18. SECURITY CLASSIFICATION OF THIS PAGE	19. SECURITY CLASSIFICATION OF ABSTRACT	20. LIMITATION OF ABSTRACT
UNCLASSIFIED	UNCLASSIFIED	UNCLASSIFIED	